Low-cost pseudolites: a loop-back time synchronization scheme for pseudolites using real-time clock offset calibration for reliable PNT

Muhammad Subhan Hameed, Mathias Philips-Blum, Thomas Pany
Universität der Bundeswehr München
Daniel Sanroma, Sowmyashree Lakshmaiah
WORK Microwave GmbH

BIOGRAPHY

Muhammad S. Hameed received his M.Sc. in Earth Oriented Space Science and Technology (ESPACE) in 2020 from the Technical University of Munich (TUM), Germany. He has been working as a research associate at the Institute of Space Technology and Space Applications of the Universität der Bundeswehr München. His current research interests include GNSS receiver technology, signal generation, tracking performance analysis and positioning using LTE signals.

Mathias Philips-Blum received his M.Sc. in Geodesy and Geoinformatics from the Leibniz University of Hannover, Germany in 2012. In 2017 he joined the Institute of Space Technology and Space Applications (ISTA) of the University of Armed Federal Forces Germany in Munich. He is currently a Ph.D. student working on algorithms for navigation in space and on Earth and on the topic of simulation of test environments.

Prof. Thomas Pany works for the University of the Bundeswehr Munich as a full professor for satellite navigation since 2016. He obtained his PhD from the Graz University of Technology in 2001 and worked in the GNSS industry for seven years. He authored around 250 publications including one monography and received five best presentation awards from the ION. He is an active member of the ION and IEEE, and he also organizes the Munich Satellite Navigation Summit. His research interests are centered around navigation signal processing, including signal design and fusion with inertial navigation.

Daniel Sanroma is a GNSS engineer at WORK Microwave involved in the development of signal generators, automated testing and software algorithms for GNSS simulators. Previously he worked among others in GPS and INS integration, in the development of a GNSS software receiver and in studies related to the EGNOS system. Daniel Sanroma earned his Master's degree in Telecommunication Engineering from the Barcelona School of Telecommunication Engineering (ETSETB).

Sowmyashree Lakshmaiah is the Director of Navigation Simulators at WORK Microwave. She is responsible for defining the product vision for the company's navigation simulator portfolio with a focus on bringing creativity to the software development process. She earned her Master's degree in Geomatics Engineering from the Technical University of Stuttgart, Germany and Bachelor degree in Electronics and Communication Engineering, India. She started her career in navigation as a GNSS Engineer in India and her main activities involved high vehicle dynamics and GNSS signal simulation.

ABSTRACT

This paper presents the development of a cost-effective pseudolite (PL) transmitter assembly capable of transmitting a GNSS-like signal for navigation. A novel loop-back time synchronization scheme is introduced, which utilizes PL pseudorange observations over a predefined cable length to achieve real-time clock offset calibration, ensuring reliable position, velocity and time (PVT) solutions. The paper details the PL signal design, transmitter hardware implementation and the loop-back time synchronization framework providing validation results using a GNSS signal simulator over pre-defined cable lengths with a RMSE within 1 m. Moreover, single point positioning (SPP) results are presented for measurement scenarios using both GNSS-only and GNSS combined with the PL signal in terms of positioning accuracy and dilution-of-precision (DOP) metrics. The combined use of the PL signal with GPS shows an overall improvement in DOP metrics and a reduction in vertical position error by approximately 3 meters. Overall, the presented transmitter architecture eliminates the need for expensive synchronization hardware and complex timing protocols and lays foundation for easily deployable ground-based PL transmitters.

I. INTRODUCTION

Interest in augmenting GNSS and exploiting alternate navigation sources has gained interest due to degradation of GNSS-only positioning in challenging reception environments such as urban canyons (Eldredge et al., 2010; O'Driscoll et al., 2011). Pseudolite (PL) transmitters, functioning as ground-deployed satellite alternatives, potentially offer a significant role in enhancing

dilution of precision (DOP) metrics and user position accuracy, given that a tight synchronization with the standard GNSS time scale is achieved (Cobb, 1997; Ma et al., 2019). The pseudolites can inherently provide an advantage of high signal reception power and a dense terrestrial network of transmitting stations, resulting in high signal availability and potential usability for navigation when GNSS signals are unavailable. Over the past decade, several PL systems have been developed, which tend to exploit different time synchronization methodologies to realize PVT. The Locata system operates a network of transceivers which transmit signals in the WiFi band and are synchronized through clock steering based on known transmitter positions (Barnes et al., 2002, 2003; Gauthier et al., 2013). TU Delft's SuperGPS (Dun et al., 2019) project employs a hybrid optical and wireless terrestrial system, synchronizing radio transmitters with a fiber optic network using the White Rabbit (Serrano et al., 2013) protocol via existing fiber optic networks. Syntony's SubWave (Gernot et al., 2020) extends GNSS coverage indoors and underground using a leak-feeder concept, injecting signals into radiating cables having axial slots acting as mini transmitters for positioning. The existing PL systems can be characterized to require dedicated receiver units, employ expensive synchronization hardware or provide zone-based positioning. This paper describes the development of a low-cost PL system, that employs a loop-back time synchronization scheme, that uses pseudorange observations over a known cable length to realize real-time clock offset calibration for reliable PVT.

Firstly, this paper describes in section II and III the hardware development of a PL transmitter assembly and the PL signal design, respectively. The transmitter assembly receives GNSS for synchronization and transmits a GNSS-like signal. The hardware concept includes a PL signal generator that generates an RF signal with a desired spreading code, pulse chip shape and navigation message modulation along with a clock module that uses a commercial GPS receiver to generate a stable frequency source and a GPS aligned pulse per second (PPS) signal to drive the signal generator and the PL receiver frontend. Secondly, based on the PL transmitter hardware, the paper describes in section IV a loop-back time synchronization scheme for tight synchronization to GNSS time base. This is achieved by looping back the generated PL signal back into the PL receiver front-end over a cable of known length allowing the PL signal to be tracked in combination with GNSS signals at the PL assembly. Thirdly, in section V, the paper presents a validation test setup and results of the loop-back scheme using a GNSS signal simulator. Lastly, section VII provides experimental acquisition and tracking results for the PL signal along with positioning results of a static receiver using both GNSS and the PL signal. The results are presented for a GNSS-only and GNSS combined with PL test cases with DOP and positioning accuracy metrics.

The presented results exhibit a proof-of-concept for pseudolite time synchronization without the need of expensive atomic clocks or sophisticated time-sharing protocols such as White Rabbit. It lays foundation for positioning using low-cost and easily deployable PL units that do not require dedicated rover receiver units for signal reception and PVT. The loop-back scheme, currently utilizing only PL pseudorange observations, can eventually be realized with carrier phase measurements in future given that the same RF front-end is used for the PL transmitter and receiver.

II. PSEUDOLITE TRANSMITTER ASSEMBLY

The PL transmitter assembly, developed in collaboration between University of Federal Armed Forces Munich (UniBW M) and WORK Microwave GmbH as part of the Firefly project, aims to achieve combined positioning using GNSS and PL signals. In this collaboration, UniBW M covered the development of the PL receiver unit, which includes a receiver front-end and software receiver, while WORK Microwave GmbH developed the hardware for the clock module and PL signal generator. The communication between the receiver and transmitter units has been realized using the UDP protocol over a physical Ethernet connection. The complete transmitter assembly is shown in Fig. 1(a).

In this setup, a receiving antenna connects to a receiver front-end, which logs IQ samples in the L1 band and provides these samples to the MuSNAT (Arizabaleta et al., 2021) software defined receiver (SDR). The MuSNAT SDR processes the IQ samples in real-time to derive time information from GNSS signals and then configures the signal generator with necessary parameters like spreading codes, signal power, bandwidth, and pulsing duty cycle. Both the receiver front-end and signal generator are driven by the clock signals from the clock module for synchronization. Once signal configuration is complete, MuSNAT sends a time configuration message, and upon receiving a trigger signal, the signal generator begins generating the PL signal at the next PPS pulse. Subsequently, MuSNAT continues to send navigation messages, which are then modulated onto the PL signal.

The hardware setup of the Firefly PL transmitter assembly is shown in Fig. 1(b). Here, the transmit antenna and the receiving antenna are mounted on a tripod stand. RF cables from both antennas connect to a box that house the receiver front end, an interface conversion box, the signal generator and clock module. The primary goal of this assembly is to transmit a GNSS-like signal, which can be used for positioning in conjunction with conventional GNSS signals. This can be achieved by using a receiver capable of successfully acquiring and tracking the pseudolight signal and decoding its navigation message to obtain navigation parameters, such as the PL transmitter's position and its clock offset.

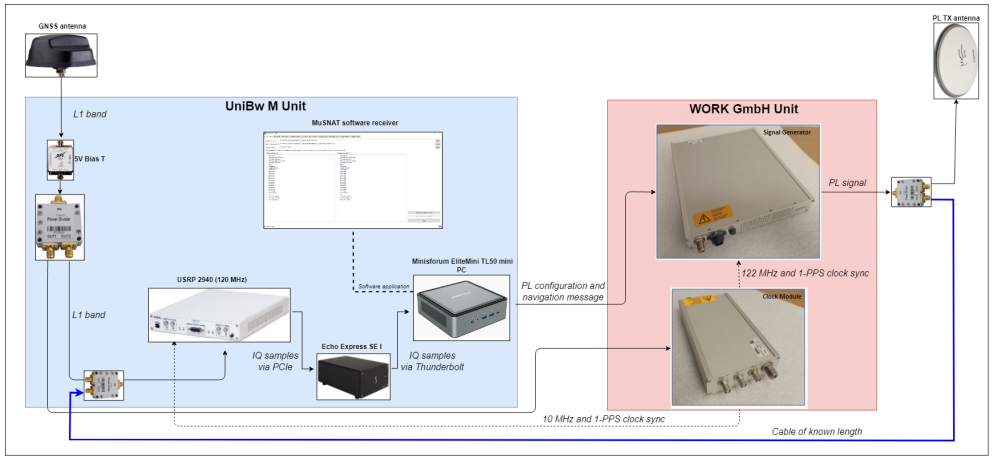

(a) Block diagram

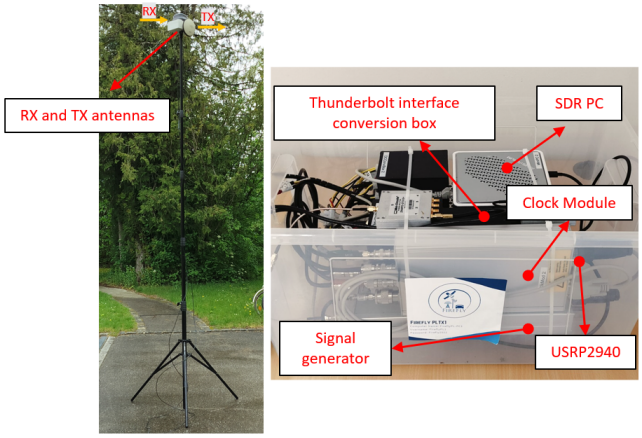

(b) Hardware setup

Figure 1: Pseudolite transmitter assembly

1. Clock module

The developed clock module, a GPS disciplined oscillator, uses an effective, high-quality, stable OCXO and a commercial GPS receiver module. The objective is to combine the low jitter of the OCXO signal with the long–term stability of a GPS signal to generate a stable frequency source (10 MHz and 122.76 MHz clock signals) and a low jitter PPS aligned to GPS. The 10 MHz and 122.76 MHz signals are used to drive the PL receiver frontend and the signal generator, respectively.

A block diagram of the clock module is shown in Fig. 2. The antenna receives GPS signals which are processed by a commercial GPS receiver, generating a 1-PPS signal aligned to the GPS time. In addition, the stable OCXO generates its own PPS. A first control loop aligns the PPS signals to produce a low jitter output PPS, while a second control loop aligns the phase of the 122.76 MHz and 10 MHz signals.

The synchronization loop is closed using a microcontroller. A phase detector is used to synchronize the PPS pulses generated by the commercial GPS receiver and the OCXO. For this purpose, a mechanism to measure the time difference between the two leading edges of the pulses is implemented. In order to synchronize the PPS signals, the microcontroller constantly reads the measured time difference and uses the result to calculate the next tuning voltage for the 10 MHz oscillator. The PPS control loop is based on a PI control scheme. For the PPS signal an update of the tuning voltage adjustment is performed. A high jitter in the input signal can cause a jump in the tuning voltage value, causing also a jump in the generated signals. In order to minimize this effect and improve the stability of the generated signal, two modifications have been implemented within the control loop for the update of the control parameters - step-wise adjustment and multi-level adjustment. Within step-wise adjustment, the tuning voltage sent to the OCXO is not updated every second and all at once, but the tuning voltage value is divided into smaller values and each of them is applied in smaller steps within one second. The multi-level adjustment aims to have an adaptive control loop depending on the incoming signal by applying multi-level adjustment to optimize reaction time and jitter. For this

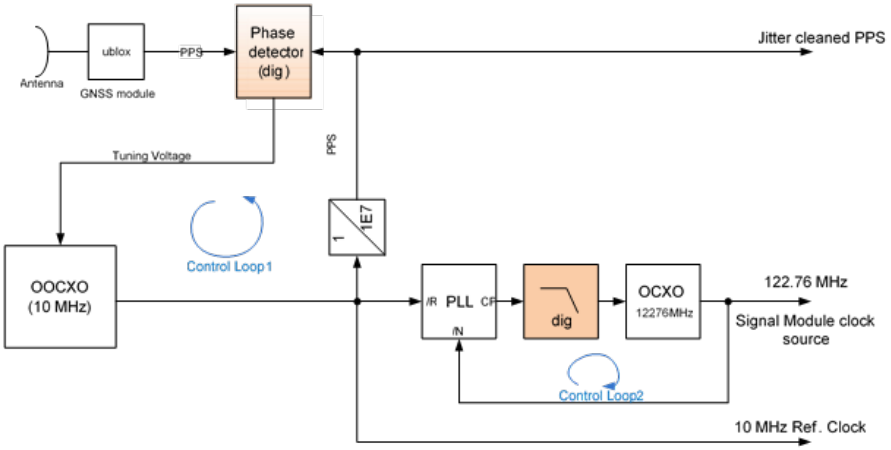

Figure 2: Clock module block diagram

purpose, different lock levels are defined, each using a set of PI coefficients. The control loop is moved to the next or to the previous level depending on certain control criterion being met or not for a predefined time interval.

Moving to lower levels means faster reaction to sudden changes in reference pulse and increase of jitter, while moving to higher levels means slower reaction to sudden changes in reference pulse and reduction of jitter. Upon initialization, the PI coefficients are set to the lowest level to get as close and fast as possible to reference pulse. The control loop moves to next higher levels if the criterion of the corresponding level are met assuring that the pulse is maintained close to reference pulse while reducing the jitter.

2. RF reception and transmission

The transmitter assembly receives GNSS signals in the L1 frequency band using a PCTEL Coach II multi-band antenna (PCTEL, 2021). The L1 band signal is then split, with one feed directed to the clock module and the other to an RF combiner. The clock module processes the L1 band GPS signals to derive time information needed to generate stable clock and PPS signals. The PL signal, generated by the signal generator, is similarly split. One feed is directed to a Novatel GPS-704-X passive transmit antenna for over-the-air transmission, while the other is looped back into the RF combiner over a cable of known length.

3. Receiver front-end

The receiver front-end is a NI USRP2940, which is driven by the 10 MHz clock signal provided by the clock module. The front-end logs L1 band signals as 16-bit IQ samples at 10 MHz sampling rate in real-time, through a proprietary LabView logging software. The software runs on an SDR on-board computer, which is connected to the front-end through a Thunderbolt 3 interface. To realize this, an interface conversion box is employed, converting the PCIe output of the USRP2940 to a Thunderbolt interface compatible with the SDR computer. The logged IQ samples are then transmitted to the MuSNAT SDR via the TCP protocol for further processing.

4. Software receiver

The MuSNAT SDR processes the logged IQ samples to acquire and track GNSS satellites deriving time information using SPP. Once a successful SPP solution is computed, the software receiver instantiates a dedicated navigation module, illustrated in Fig. 3(a), which establishes communication with the signal generator hardware. The navigation module hosts a UDP server, initiating a handshake protocol with the signal generator over its client IP address.

After a successful handshake between the SDR and the signal generator, the system adopts a finite state machine (FSM) control logic, as illustrated in Fig. 3(b). The FSM begins with the SDR querying the status of the signal generator, which can respond with one of three statuses: *Inactive*, *Initialized* or *Ready*. Upon receiving an *Initialized* status, the FSM transitions to the second state, where the SDR sends a signal configuration message to the signal generator. This configuration message includes key parameters such as the complete primary and secondary codes as well as a set of RF parameters, including signal frequency, transmit power, bandwidth, and pulse duty-cycle. The signal generator then uses these RF parameters to configure an L1 carrier signal and applies BOC(1,1) modulation onto the provided spreading codes.

Following the signal configuration, control returns to the initial state, where the FSM awaits a *Ready* status from the signal generator. Upon receiving this status, the FSM advances to the third state. In this state, the SDR transmits a start time configuration message, which specifies the precise time of the epoch at which the signal generator should begin transmitting the PL signal. As the SDR enters this state, it begins comparing the current time with the specified start time, calculating the time difference in seconds. Concurrently, the SDR starts a parallel thread that periodically sends fully encoded navigation messages to the signal generator at each message period. When the time difference between the current epoch and the start time is less than one second, the SDR sends a soft trigger message to the signal generator. This trigger instructs the signal generator to initiate signal generation and transmission precisely at the rising edge of the next PPS pulse.

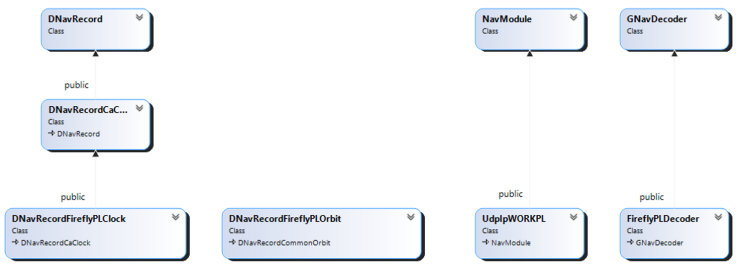

(a) MuSNAT PL navigation module class diagram

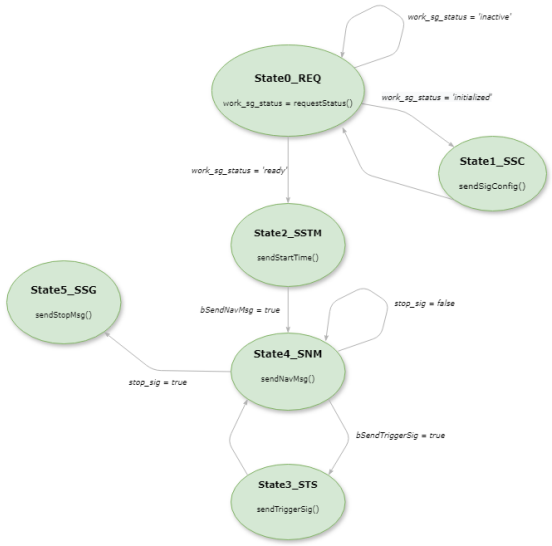

(b) FSM for pseudolite control logic

Figure 3: SDR development for pseudolite signal

5. Pseudolite signal generator

The FPGA-based signal generator has been developed to allow flexible signal generation of signals in the E1 and E6 GNSS bands. The block diagram of the signal generated is shown in Fig. 4(a). The FPGA is a Xilinx XCKU15P with a MicroBlaze soft microcontroller core. An Ethernet interface allows the communication via UDP protocol between the navigation module and the signal generator. A proprietary UDP protocol has been defined to communicate messages used for configuration and control of the generator as well as a soft trigger message to initiate signal generation. The received messages are serialized and converted to UART protocol. The UART messages handling including message parsing, integrity checks, response management or database control is performed by the MicroBlaze. Once the incoming messages are processed by the MicroBlaze, it also distributes them to the corresponding end nodes of the FPGA. The configuration parameters are passed to an IP core which writes the values in control registers used by different IP cores for the generation of the PL signal. Once the signal generator is triggered, the incoming navigation data is forwarded to a navigation data first-in first-out (FIFO) buffer. The navigation data is then combined with the PRN codes. There are three different PRN generators connected in cascade, allowing the generation of primary, secondary and non-memory codes. The PRN encoded data bytes from the PRN generator are passed to the modulator, which maps them to the corresponding phase states using a look-up table (LUT). The digital baseband signal is then generated by converting the phase states into values for the I and Q channels. FIR filters are also implemented within the FPGA allowing to limit the bandwidth of the PL signal by configuration. The digital baseband signal is then passed to a dual RF digital-to-analogue converter (DAC) controlled by the FPGA via a JESD204B interface and the RF signal is generated.

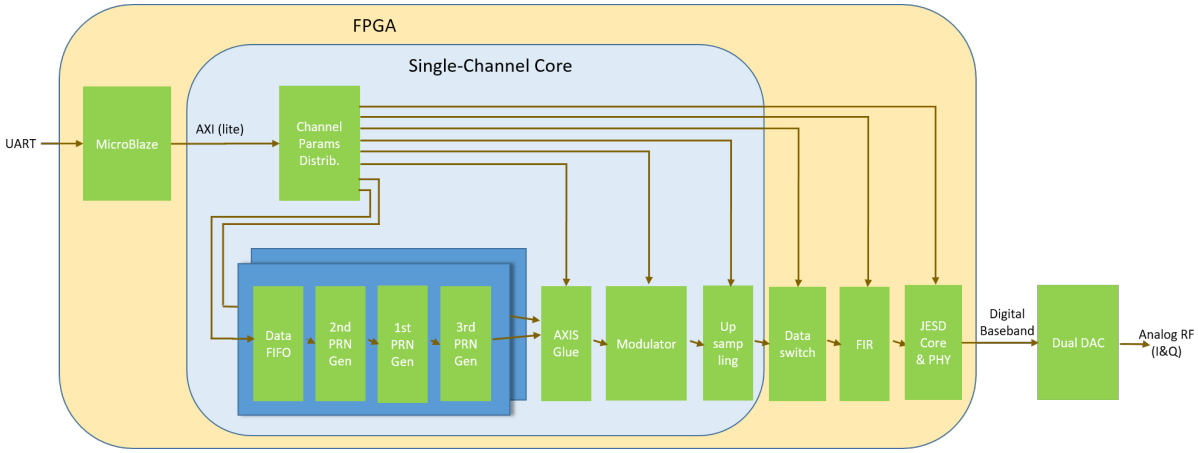

(a) Block diagram

(b) Front Panel View

(c) Rear Panel View

Figure 4: Pseudolite signal generator

III. PSEUDOLITE SIGNAL STUCTURE

This section provides an overview of the PL signal structure, specifically designed for transmission at the L1 frequency band as a PL E1BC signal, including its modulation scheme, spreading codes, and message format.

1. Spreading codes and modulation

The ranging codes for the PL signal adopt a tiered code approach, which incorporates both primary and secondary codes. The spreading codes are derived from the Galileo E1BC code family, utilizing four distinct PRNs ranging from 45 to 50. To reduce cross-correlation with Galileo E1BC satellites currently visible in the sky, these codes are time-wise flipped. The signal is divided into two components: the Data and Pilot components. The Data component is modulated using the primary codes and includes navigation message, while the Pilot component is modulated with both primary and secondary codes but does not carry navigation messages. The primary codes are further modulated with BOC(1,1) subcarrier.

2. Navigation message

The navigation message employed in the PL signal is based on the INAV message structure of Galileo E1B, as specified in the Galileo Signal In Space Interface Control Document (European-Commission, 2010). This message format incorporates the Dummy Word, shown in Fig. 5(a), which is utilized to include a proprietary format message structured to define the navigation parameters specific to the PL signal. The proprietary format, expressed as the Dummy Sequence, encodes essential information such as the PL's position and clock correction parameters. This adaptation ensures compatibility with existing Galileo systems while providing the necessary enhancements for pseudolite-based navigation.

The proprietary frame structure of the Dummy Sequence is shown Fig. 5(b). It includes the Signal Send Time, which is represented by the Time of Week (TOW) in seconds and the Week Number, the position of the PL transmitter in meters within the earth-centered earth-fixed (ECEF) coordinate system, the PL clock offset in seconds, and the positions of cellular LTE transmitters that shall be visible to both the PL receiver and a ground rover. The inclusion of LTE transmitter positions, for potentially trackable cellular base stations, aims to aid in using LTE signals as signal of opportunity for navigation as highlighted

in (Hameed et al., 2022; Arizabaleta-Diez et al., 2022; Hameed et al., 2023b,a). A rover receiver, when equipped with a decoder for the PL navigation message, can use these navigation parameters to perform positioning. The position of the PL can be determined with high precision using geodetic methods for static applications or estimated in real time through real-time kinematic (RTK) or SPP techniques. The clock correction parameter is estimated using a loop-back scheme as described in section IV.

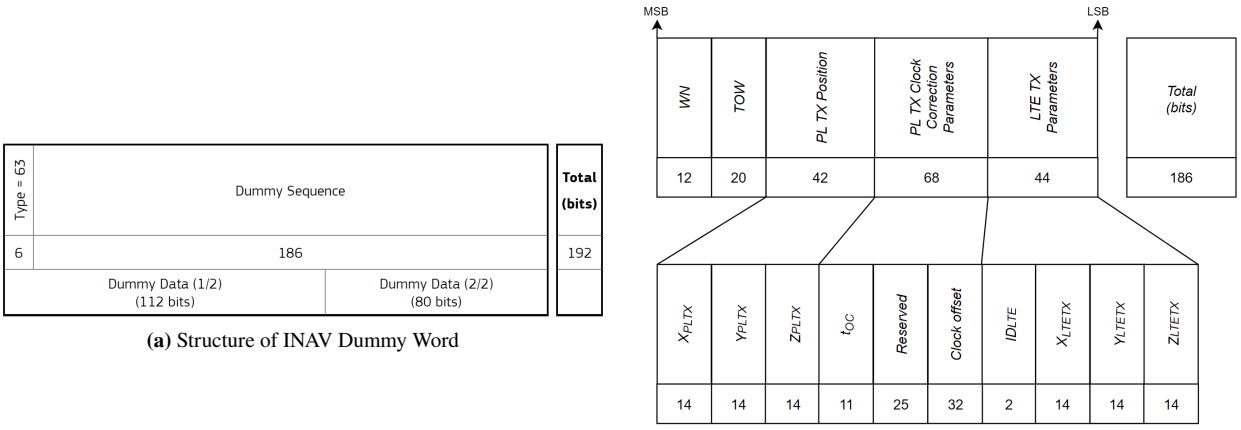

(a) Structure of INAV Dummy Word

(b) Dummy sequence as PL navigation message format

Figure 5: PL navigation message structure

IV. LOOP-BACK SYNCHRONIZATION SCHEME

The loop-back time synchronization scheme, depicted in Fig. 6, describes a method for synchronizing the PL transmitter with the GNSS time base. In this scheme, the PL signal generated by the signal generator is looped back into the PL receiver front-end over a cable of precisely known length, indicated by the solid blue line. This loop-back connection allows for the direct measurement of the pseudorange of the PL signal. As both the PL signal generator and the receiver front-end are driven by clock signals produced by the same clock source, they are inherently synchronized. The loop-back scheme leverages this synchronization facilitating run-time calibration of the system.

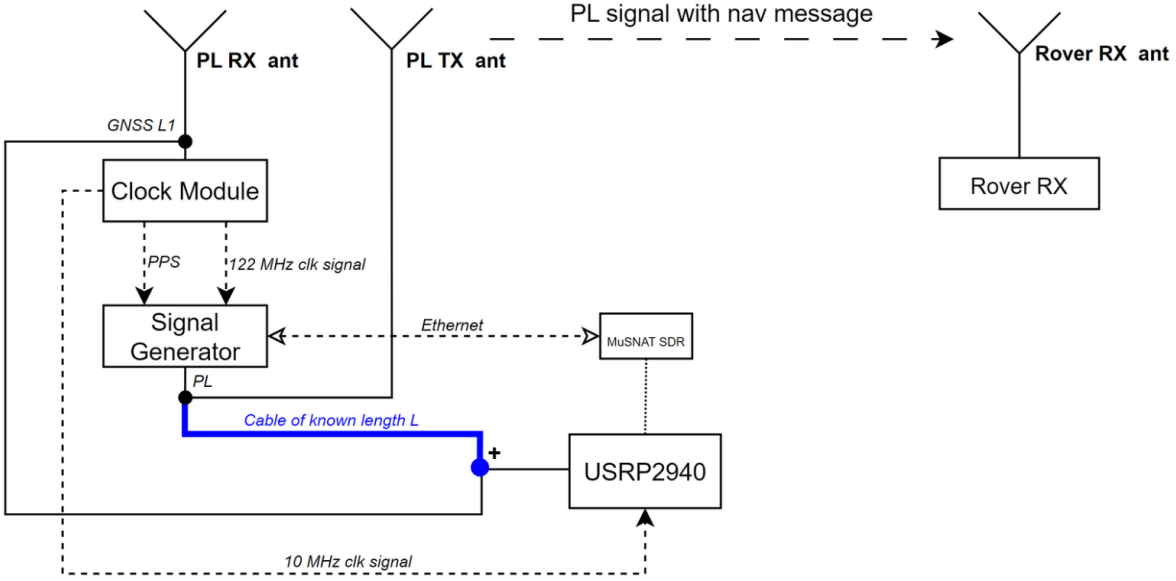

Figure 6: Block diagram illustrating the loop-back synchronization scheme

With this synchronization established, the PL pseudorange ${\rho_r}^{PL}$ as received at the PL receiver r can be expressed as shown in (1). Here, with respect to GNSS time base, $\delta\tau_r$ is the receiver clock offset, $\delta\tau^{PL}$ is the transmitter clock offset, B_r is the receiver code bias, B^{PL} is the transmitter code bias and c is the speed of light. The signal travel is determined by the physical length L_{PL} and the velocity factor κ_{PL} of the loop-back cable. The measurement noise is denoted by η_r^{PL}.

In a physical cable, the RF signal travels at a speed less than the speed of light in free space and which is determined by its velocity factor. The velocity factor is defined as the ratio of the speed at which a wavefront of the radio signal passes through the medium, to the speed of light in vacuum, constituting a different electrical length of the transmission medium than its physical length (Gottlieb, 1993). The difference is accounted for by dividing the physical length of the loop-back cable L_{PL} by its velocity factor κ_{PL} in (1).

To minimize the effect of hardware code biases, the loop-back scheme operates over a single-frequency system where differential code biases do not contribute in PVT error. The absolute delay in signal propagation from the receiver antenna phase center to the digital channels can be substantial, potentially exceeding 1 μs, particularly with long antenna cables or with the use of sophisticated analogue filters. However, within such a setup, for signals on the same carrier frequency, it is considered that all visible signals are delayed by the same common delay (Kaplan and Hegarty, 2017). The common delay, hence, does not affect the positioning accuracy and is primarily reflected in the least-squares estimate of the receiver's clock bias. Overall, it is to note that the scheme does not particularly depend on an accurate estimate of the actual receiver clock offset but rather on the estimation and elimination of the absolute receiver delay represented by the sum of receiver clock offset $\delta\tau_r$ and hardware delay B_r as shown in (2).

The absolute receiver delay $\widetilde{\delta\tau_r}$ can be estimated using GNSS using least-mean-squares and then used to correct the PL pseudorange measurements. The absolute transmitter delay can similarly be parameterized in terms of the actual transmitter clock offset $\delta\tau^{PL}$ and the transmitter hardware delay B^{PL} as shown in (3). To solve for the absolute transmitter delay $\widetilde{\delta\tau}^{PL}$, the known travel time of the signal through the loop-back cable is subtracted from a temporal mean value of the corrected pseudorange as shown in (4) with a window size of N. This difference provides an estimate which can be broadcast within the PL navigation message, enabling a rover receiver to utilize it for precise PVT. Incorporating the absolute transmitter delay into the navigation message enables the system to function similarly to a GNSS user segment, eliminating the need for complex hardware or timing protocols to use the signal for navigation.

$$ {\rho_r}^{PL} = \frac{L_{PL}}{\kappa_{PL}} + c\left(\delta\tau_r - \delta\tau^{PL} + B_r - B^{PL}\right) + \eta_r^{PL} \tag{1} $$

$$ \widetilde{\delta\tau_r} = \delta\tau_r + B_r \tag{2} $$

$$ \widetilde{\delta\tau}^{PL} = \delta\tau^{PL} + B^{PL} \tag{3} $$

$$ \widehat{c\delta\tau}^{PL} = \frac{L_{PL}}{\kappa_{PL}} - \frac{1}{N}\sum_{i=0}^{N}\left({\rho_{r,i}}^{PL} - \widehat{c\delta\tau_r}\right) + \eta_r^{PL} \tag{4} $$

V. VALIDATION WITH GNSS SIGNAL SIMULATOR

This section describes a validation exercise conducted to assess the loop-back synchronization scheme using a Rohde & Schwarz SMW200A GNSS signal simulator. The goal of this validation was to obtain precise range measurements of the PL signal over cables of known lengths. The experimental setup, illustrated in Fig. 7(a), employs the R&S simulator generating an L1 signal with GPS L1 CA satellites with no atmospheric delays. This signal is directed to the clock module, the PL receiver front end, and a rover receiver front end. The rover front-end is driven by its own internal OCXO clock and is hence not inherently synchronized with the PL transmitter assembly.

The PL transmitter uses the loop-back synchronization scheme to estimate its clock offset, which is broadcast in the PL signal navigation message. The rover receives both the GPS and PL signals. Using GPS-only observations, the rover estimates its own clock offset as well as decodes the PL navigation message to obtain the PL transmitter clock offset and applies these to the PL pseudorange observations. The corrected PL range measurements are subsequently compared to the actual cable length that extends from the signal generator's output to the RF combiner of the rover receiver front end. This comparison facilitates an evaluation of the accuracy and effectiveness of the PL transmitter's clock estimation.

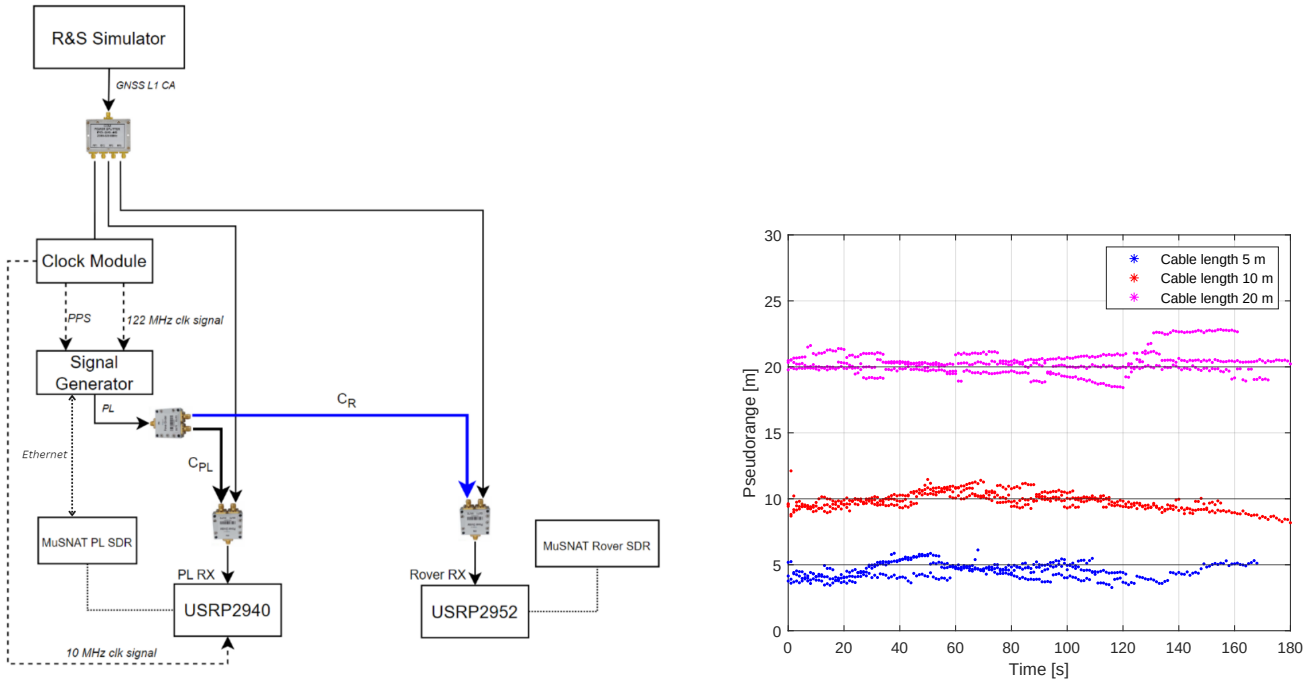

(a) Validation setup

(b) Validation results

Figure 7: Validation of loop-back scheme with R&S simulator

At the rover end, to establish an accurate relationship between the received PL pseudoranges and the actual signal propagation cable length, the velocity factors of individual PL cable segments are required to be considered. In (5), the observation model for the PL pseudorange ${\rho_R}^{PL}$ at the rover receiver R is shown where $\widetilde{\delta\tau_R}$ is the rover receiver clock offset, $\widetilde{\delta\tau^{PL}}$ is the PL transmitter clock offset and c is the speed of light. The clock offset terms are assumed to absorb the hardware delays. The signal travel is determined by the physical length L_R and the velocity factor κ_R of the loop-back cable. The measurement noise is denoted by η_R^{PL}.

It is worthwhile to note that both (1) and (5) are parameterized in terms of the cable velocity factor κ to account for the electrical length of the cable within the pseudorange observations. This can as well be achieved alternatively by modeling the observations using only the physical lengths and by adjusting the rover pseudoranges at the measurement level. This is expressed in (6) where ${\bar{\rho_R}}^{PL}$ is the pseudorange considering only the physical length of the rover cable.

$$ {\rho_R}^{PL} = \frac{L_R}{\kappa_R} + c\left(\widetilde{\delta\tau_R} - \widetilde{\delta\tau}^{PL}\right) + \eta_R^{PL} \tag{5} $$

$$ {\rho_R}^{PL} = \frac{{\bar{\rho_R}}^{PL}}{\kappa_R} + \left(\frac{L_{PL}}{\kappa_{PL}} - L_{PL}\right) \tag{6} $$

Table 1 outlines the specifications of the coaxial cables used for the PL signal. Within the setup shown in Fig. 7(a), the PL loop-back cable C_{PL}, which extends from the RF splitter at the output of the signal generator to the RF combiner at the input of USRP2940, is selected to be of coaxial type Aircell 7 (SSB-Electronic-GmbH, 2023) with a length L_{PL} = 20 m and velocity factor $\kappa_{PL} = 0.85$. The rover cable C_R, which extends from the RF splitter at the output of the signal generator to the RF combiner at the input of USRP2952, is selected to be type RG58 C/U with a velocity factor $\kappa_R = 0.66$. Three different lengths are considered for the rover cable. Within the SDR processing of both the PL and rover ends, the physical lengths of the cables are considerd. Hence, to account for the difference in electrical and physical lengths of both C_{PL} and C_R, the PL pseudorange logged by the rover SDR is expressed as ${\bar{\rho_R}}^{PL}$ in (6).

With the aforementioned validation setup, three independent datasets were recorded for each cable length of C_R. For each dataset, the PL pseudoranges, as logged in the MuSNAT SDR RINEX file, were obtained and the relationship shown in (6) was used to solve for ${\rho_R}^{PL}$. Fig. 7(b) shows the results of obtained pseudoranges for time duration of 180 s. Overall, it can be seen

Table 1: RF cable specifications

Parameter	C_{PL}	C_R
Cable type	Coaxial Aircell 7	Coaxial RG58 C/U
Velocity factor κ	0.85	0.66
Physical length	20 m	5 m, 10 m, 20 m

that the pseudoranges bound to a mean value approximately equal to the cable length. Table 2 shows the root mean square error (RMSE) and standard deviations of the pseudoranges for each cable length. The RMSE is at 1 m level indicating an accurate estimate of the transmitter clock offset.

Table 2: Validation results

Cable C_R	**RMSE [m]**	**Std. dev [m]**
5 m	0.727	0.560
10 m	0.643	0.572
20 m	0.806	0.733

As observable, there as well exist variations up to a meter level along with abrupt jumps within the rover pseudoranges. These variations are addressed by considering Fig. 8 which illustrates three datasets for a cable length of 20 m, where the pseudoranges at the rover SDR are shown in magenta, the demeaned measured clock offset at the PL SDR is shown in black, the measured Doppler at the PL SDR is shown in blue and the demeaned, time-averaged pseudorange at the PL SDR is represented in red. There exists high correlation between the envelopes of the pseudoranges at rover SDR and the PL SDR. This inherently implies that the variations are sourced within the PL SDR. One possible reason of these variations can be accounted to a short-term misalignment between the 10 MHz and 122.76 MHz clock signals. If the clock signals driving the PL receiver front-end and signal generator are not tightly synchronized then this would contribute in a variation within the pseudorange. It is also possible that the commercial receiver within the clock module and the SDRs estimate the receiver clock error by employing different algorithms yielding variations between the receiver time scales. Moreover, the jumps within the rover side pseudoranges could be accounted to jumps made within the clock signals for readjustment of control loop 2. These jumps are also observable within the measured Doppler time series of the PL signal at the PL SDR. In view of this, further investigation is needed to achieve a smooth PL pseudorange, as expected for this test setup.

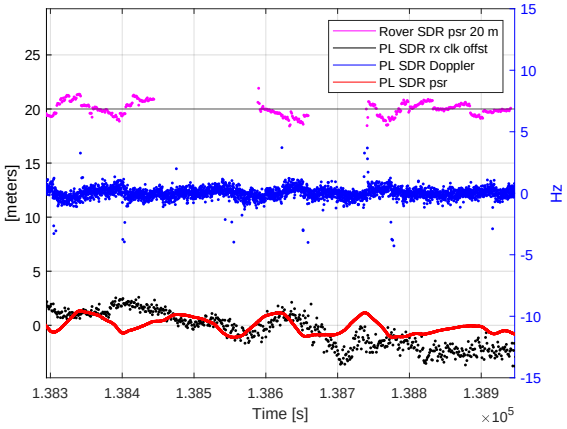

Figure 8: Variations within three time separate datasets for 20 m cable

VI. EXPERIMENTAL SETUP

This section describes the experimental setup for receiving combined GNSS and PL signals for positioning on a static receiver. In Fig. 9 the locations of the transmitter and static rover receiver are shown. The PL transmitter antenna, marked in red, is positioned on the rooftop of the UniBw M ISTA building and the static receiver antenna, marked in cyan, is located on the rooftop of another building with the RTK range between the two antennas being approximately 113 m. The PL signal synchronization is achieved through the loop-back synchronization scheme described in Section IV.

The PL transmitter is configured to generate a signal with a 40 MHz bandwidth, operating in continuous mode without

pulsing. The RF output power is set to -18 dBm at the signal generator's output. The precise coordinates of the transmit antenna, determined through post-processed RTK measurements, serve as the transmitter position modulated within the signal's navigation message. The signal is assigned PRN47. At the static receiver end, three datasets are recorded on different days, logging 16-bit IQ samples at the L1 frequency while the PL transmitter is in operation. Each dataset is subsequently post-processed using the MuSNAT SDR twice, with the SPP module initially configured to use only GPS signals and then reconfigured to incorporate both GPS and PL signals for the second run.

The following section presents the acquisition and tracking results of the PL signal, followed by an analysis of the obtained positioning results. The horizontal and vertical positioning accuracy is evaluated against the RTK coordinates of the rover antenna to assess the performance and effectiveness of the combined GNSS and PL positioning system.

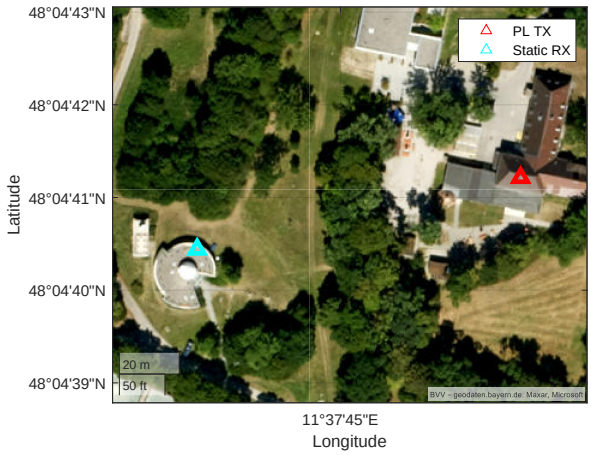

Figure 9: Experimental setup for over-the-air PL transmission

VII. RESULTS

1. Acquisition and tracking

Table 3 provides a summary of the acquisition and tracking parameters configured within MuSNAT SDR for receiving the PL signal. The signal acquisition is performed using both coherent and non-coherent methods, with an acquisition threshold set to 25 dB-Hz. For tracking the signal code, a delay lock loop (DLL) is utilized with a second order loop filter and a noise bandwidth of 1 Hz. To rectify any false side-peak tracking of the BOC(1,1) correlation function, a Bump-Jump algorithm is employed. The secondary code on the Pilot component is tracked using a combination of Viterbi decoder and Kalman Filter implemented within the SDR. The carrier is tracked using alternation between a second-order frequency lock loop (FLL) and a second-order phase lock loop (PLL), with noise bandwidths of 50 Hz and 1 Hz, respectively.

Table 3: Tracking parameters

Parameter	Value
Number of coherent acquisitions	2
Number of non-coherent acquisitions	20
Acquisition threshold [dB-Hz]	35
DLL noise bandwidth [Hz]	1
PLL noise bandwidth [Hz]	50
FLL noise bandwidth [Hz]	1

Fig.10 presents the tracking results of the PL signal captured over-the-air. Fig. 10(b) displays the In-phase (I) and Quadrature-phase (Q) tracking power. Two notable observations can be made from this figure: First, the In-phase power for the Data component exhibits the presence of navigation message symbols. To extract the PL navigation parameters, an adapted INAV message decoder is applied to these symbols to obtain PL navigation parameters. Second, the In-phase power of the Pilot component initially shows the secondary code symbols for the early epochs of the tracking period. Subsequently, there is a removal of these secondary code symbols, indicating a successful secondary code wipe-off.

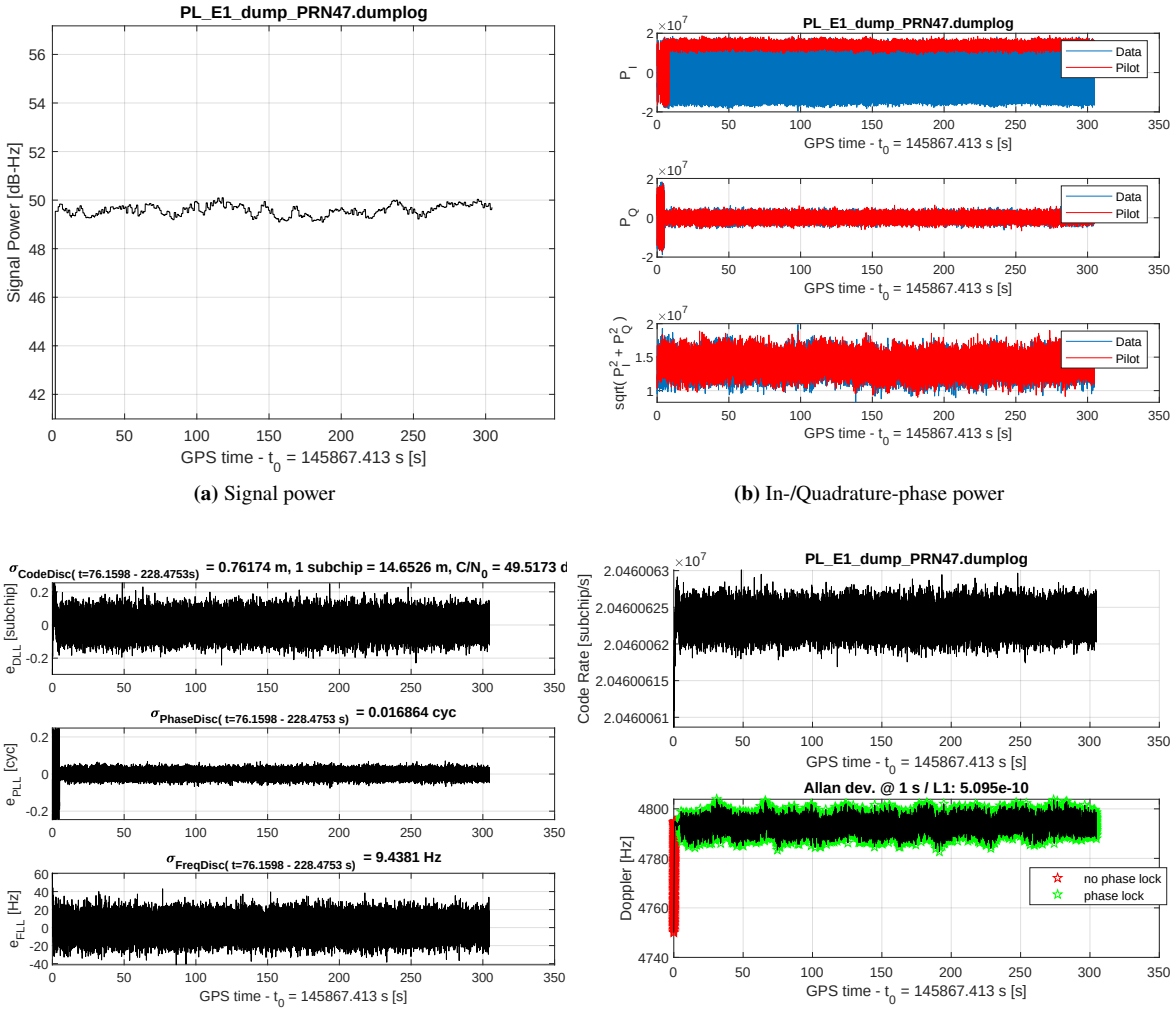

(a) Signal power

(b) In-/Quadrature-phase power

(c) Loop discriminator time series

(d) Code rate and Doppler

Figure 10: Pseudolite tracking results

Fig.10(a) shows the received signal power, which is observed to be approximately 50 dB-Hz. The signal strength indicates a strong reception of the PL signal under the experimental conditions. In Fig.10(c), the time series of the DLL, PLL and FLL discriminators are shown. The results indicate stable tracking performance, with a DLL discriminator standard deviation of 0.762 m, a PLL discriminator standard deviation of 0.0169 cycles, and an FLL discriminator standard deviation of 9.43 Hz. These metrics reflect a stable and reliable signal tracking. Finally, Fig.10(d) displays the tracked code rate and Doppler frequency. The measured Doppler shows a non-zero value, primarily due to the receiver clock offset. However, the Doppler trend remains stable and non-progressing, consistent with the fact that both the transmitter and receiver are stationary during the experiment.

2. Positioning results

Fig. 11-13 show the positioning results of datasets 1, 2 and 3 respectively for GPS-only along with combined GPS and PL test cases. Fig. 11(a)-13(a) show the number of signals used in SPP and the DOP metrics. Overall it can be observed that with the inclusion of the PL signal the DOP metrics improve indicating a better distribution of transmitters around the receiving antenna.

Fig. 11(b),(c)-13(b),(c) show the horizontal and vertical position error results which are summarized in Table 4. The RMSE values for each dataset serve as a baseline for comparative analysis. The data reveal that for datasets 1 and 2, the addition of the PL signal significantly enhances vertical accuracy, reducing the vertical RMSE from 8.130 m to 5.250 m in dataset 1 and from 11.892 m to 8.610 m in dataset 2. This improvement can be accounted to the enhancement in the vertical dilution of precision

(VDOP), indicating that ground-based PL systems can effectively improve the vertical accuracy of GNSS-based PVT solutions. However, the inclusion of the PL signal results in a slight increase in RMSE for the horizontal East and North components. This increase may be attributed to the limited precision in the averaged PL transmitter clock offset, which depends heavily on the accuracy of the estimated receiver clock offset within the PL receiver. The impact on horizontal accuracy is more pronounced due to the absence of a significant improvement in the horizontal dilution of precision (HDOP). It is anticipated that with more transmitters strategically placed around the receiver, a notable enhancement in HDOP could also be achieved.

For dataset 3, the PL signal demonstrates a significant improvement in the time-to-first-fix (TTFF). In the GPS-only case, no SPP solution is computed for the first 140 seconds, whereas, in the GPS and PL combined case, an SPP solution is obtained from the beginning. This finding underscores the potential of PL transmitters in scenarios where GNSS signal visibility is limited due to environmental constraints.

Table 4: Positioning results

Dataset	**RMSE GPS-only**			**RMSE GPS and Pseudolite**		
	East [m]	**North [m]**	**Up [m]**	**East [m]**	**North [m]**	**Up [m]**
1	2.212	0.860	8.130	2.862	1.890	5.250
2	1.178	3.091	11.892	2.184	3.705	8.610
3	2.460	2.275	4.922	2.748	3.030	6.312

VIII. CONCLUSIONS

In this paper, a low-cost PL architecture has been presented which employs a loop-back time synchronization scheme. The implementation of such a scheme eliminates the need for expensive time-sharing protocols or two-way transmission for clock steering, making it both cost-effective and simple to deploy for large-scale commercial use. A navigation system using such pseudolites relies on independent PL nodes where each node should have visibility to GNSS for retrieving time. The GNSS-like signal generated by the system requires no hardware modifications at the rover end, only minimal software upgrades, ensuring compatibility with existing navigation systems.

The results from the validation exercise indicate that the PL signal can be used by a rover, which is driven by an independent clock, to do combined GNSS and PL PVT. The results overall indicate a pseudorange variation at the meter level for the validation test setup. Moreover, the system's performance is strongly dependent on the quality of the receiver clock offset estimated at the pseudolite end. This can be ensured using advanced signal processing methods.

Experimental over-the-air positioning results for a static receiver show an improvement in the overall DOP metrics as well as a reduction in the vertical position error. Furthermore, an improvement in the TTFF is noted, by using the PL, for a test case where less GNSS satellites are acquired at the start.

The system can as well be adapted to dynamic environments, such as the use of UAV pseudolites, which has already been demonstrated or the use as a hosted LEO-PNT payload. Future versions of the system could benefit from incorporating carrier phase measurements, leveraging low-noise carrier phase observations to improve the precision of range measurements over the cable.

Overall, this approach presents a promising, scalable, and cost-effective solution for enhancing GNSS-based positioning systems, particularly in scenarios where pseudolites are required.

ACKNOWLEDGEMENTS

This work was carried out at Institute of Space Technology and Space Applications (ISTA) at Universität der Bundeswehr München as part of the project *Firefly - Mobiles und vernetztes Positionierungssystem zur gestützten Navigation in urbanen Umgebungen*, funded by the German Federal Ministry for Economic Affairs and Energy (BMWi) and administered by the project Management Agency for Aeronautics Research of the German Space Agency (DLR) in Bonn, Germany (grant no. 50NA2102).

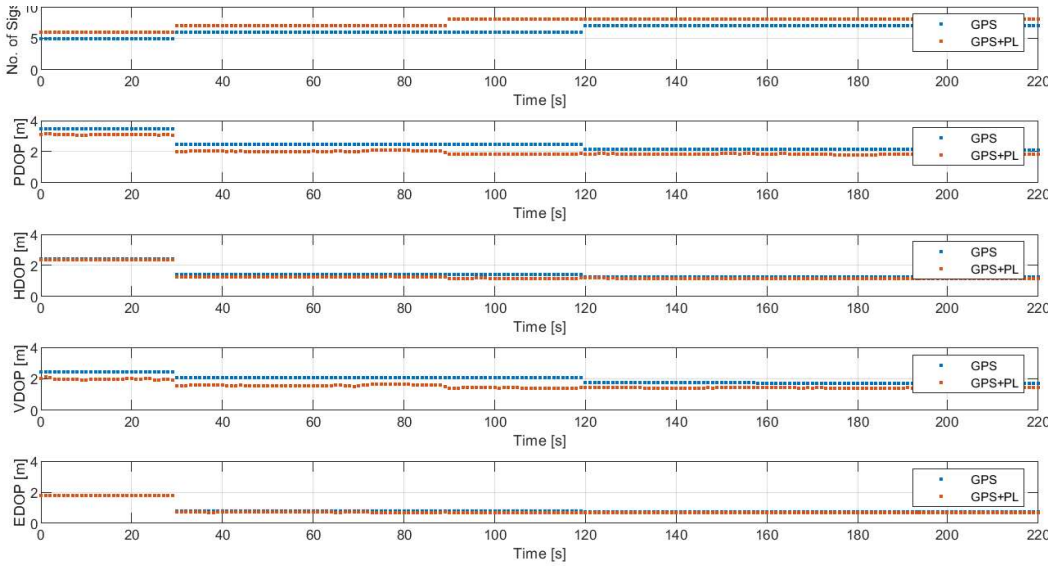

(a) DOP Metrics

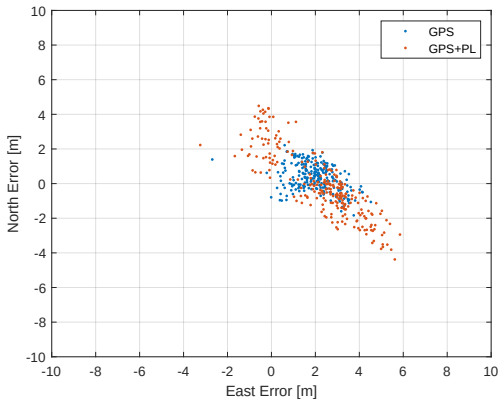

(b) Horizontal Error

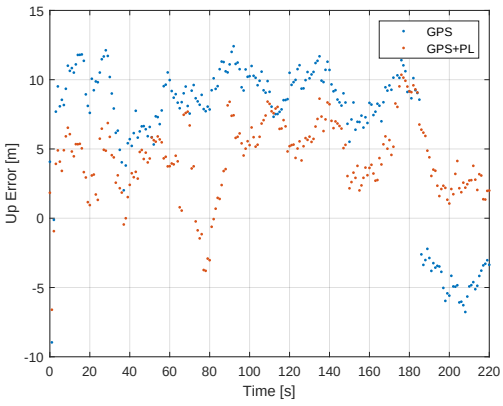

(c) Vertical Error

Figure 11: Positioning results dataset 1

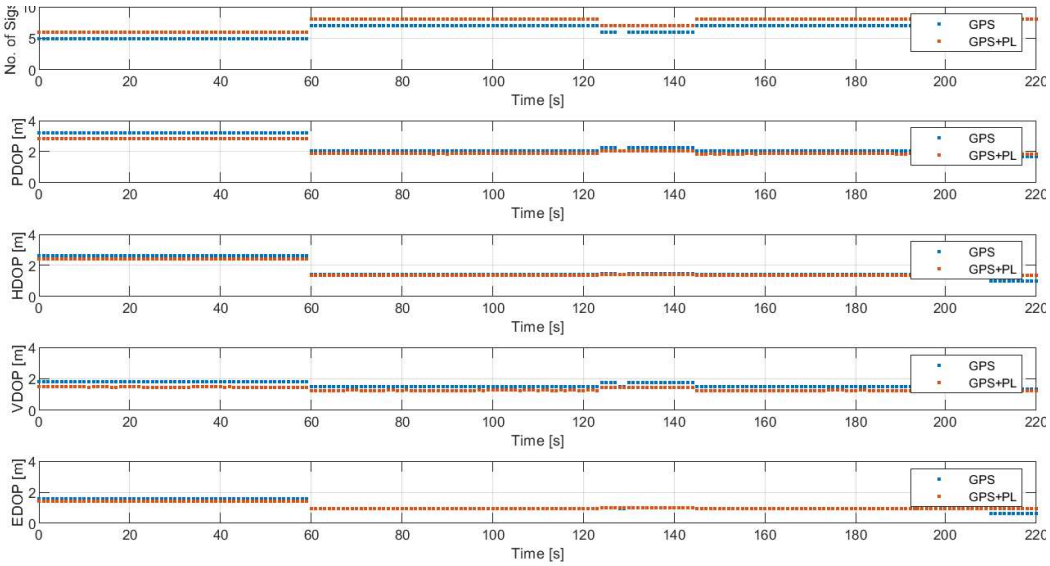

(a) DOP Metrics

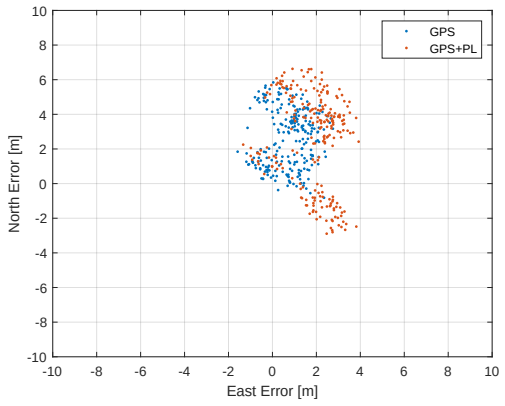

(b) Horizontal Error

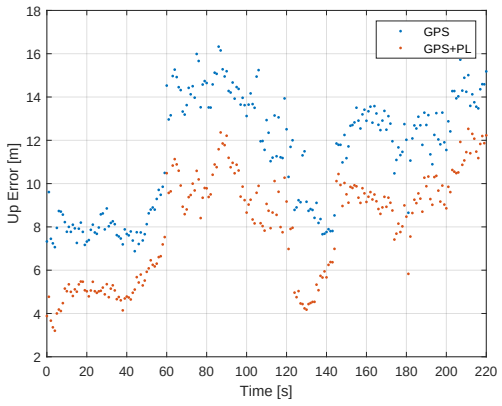

(c) Vertical Error

Figure 12: Positioning results dataset 2

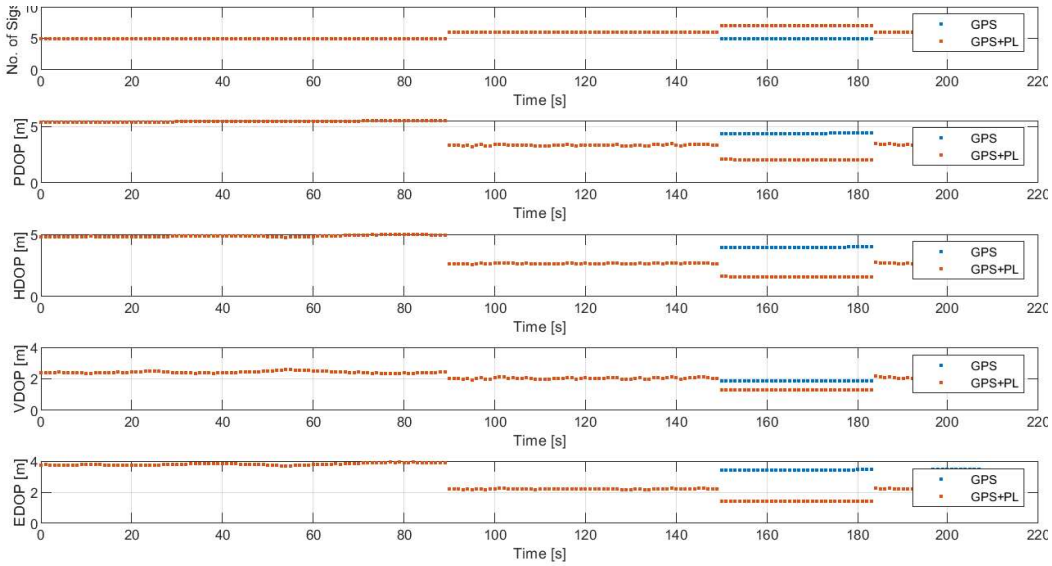

(a) DOP Metrics

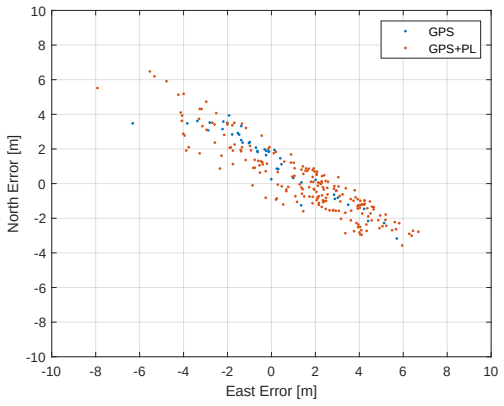

(b) Horizontal Error

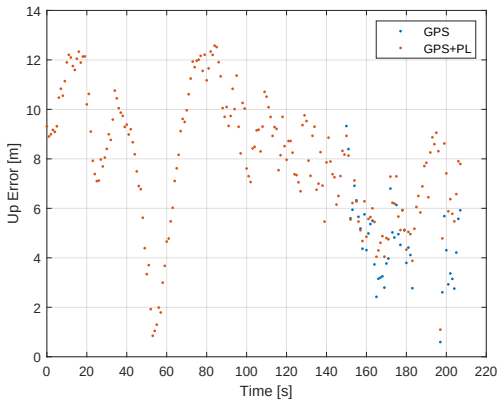

(c) Vertical Error

Figure 13: Positioning results dataset 3

REFERENCES

Arizabaleta, M., Ernest, H., Dampf, J., Kraus, T., Sanchez-Morales, D., Dötterböck, D., Schütz, A., and Pany, T. (2021). Recent enhancements of the multi-sensor navigation analysis tool (MuSNAT). In *Proceedings of the 34th International Technical Meeting of the Satellite Division of The Institute of Navigation (ION GNSS+ 2021)*, pages 2733–2753.

Arizabaleta-Diez, M., Hameed, M. S., and Pany, T. (2022). LTE transmitter location and clock state estimation: Simulated and real measurements using the SSS and CRS signals. In *Proceedings of the 35th International Technical Meeting of the Satellite Division of The Institute of Navigation (ION GNSS+ 2022)*, pages 2444–2463.

Barnes, J., Rizos, C., Wang, J., Small, D., Voigt, G., and Gambale, N. (2003). Locata: A new positioning technology for high precision indoor and outdoor positioning. In *Proceedings of the 16th International Technical Meeting of the Satellite Division of the Institute of Navigation (ION GPS/GNSS 2003)*, pages 1119–1128.

Barnes, J., Rizos, C., Wang, J., Small, D., Voigt, G., Gambale, N., et al. (2002). High precision indoor and outdoor positioning using locatanet. *Positioning*, 1(05).

Cobb, H. S. (1997). *GPS pseudolites: Theory, design, and applications*. Stanford University.

Dun, H., Tiberius, C. C., Janssen, G. J., and Diouf, C. (2019). Time delay estimation based on multi-band multi-carrier signal in multipath environments. In *Proceedings of the 32nd International Technical Meeting of the Satellite Division of The Institute of Navigation (ION GNSS+ 2019)*, pages 2299–2313.

Eldredge, L., Enge, P., Harrison, M., Kenagy, R., Lilly, R., Lo, S., Loh, R., Narins, M., and Niles, R. (2010). Gnss vulnerability and alternative pnt. *GPS World*, 21:38–39.

European-Commission (2010). *European GNSS (Galileo) Open Service Signal In Space Interface Control Document*. Publications Office.

Gauthier, J. P., Glennon, E. P., Rizos, C. C., and Dempster, A. G. (2013). Time transfer performance of locata–initial results. In *Proceedings of the 45th annual precise time and time interval systems and applications meeting*, pages 150–157.

Gernot, C., Gernot, F., and Patout, B. (2020). Positioning system with means of generating gnss signals and radiating cable. US Patent 10,739,472.

Gottlieb, I. M. (1993). *Practical RF power design techniques*. TAB/Electronics.

Hameed, M. S., Arizabaleta-Diez, M., and Pany, T. (2022). LTE transmitter position estimation through combined GNSS and LTE tracking using a software receiver.

Hameed, M. S., Arizabaleta-Diez, M., Philips-Blum, M., Dötterböck, D., and Pany, T. (2023a). Precise lte transmitter localization using crs carrier phase tracking with an on-board atomic clock and lte double-difference observations. In *Proceedings of the 36th International Technical Meeting of the Satellite Division of The Institute of Navigation (ION GNSS+ 2023)*, pages 2431–2449.

Hameed, M. S., Philips-Blum, M., Arizabaleta-Diez, M., and Pany, T. (2023b). Lte transmitter states estimation using a combined code and carrier phase observation model. In *2023 IEEE/ION Position, Location and Navigation Symposium (PLANS)*, pages 1107–1117. IEEE.

Kaplan, E. D. and Hegarty, C. (2017). *Understanding GPS/GNSS: principles and applications*. Artech house.

Ma, C., Yang, J., Chen, J., and Tang, Y. (2019). Time synchronization requirement of global navigation satellite system augmentation system based on pseudolite. *Measurement and Control*, 52(3-4):303–313.

O'Driscoll, C., Borio, D., Fortuny, J., et al. (2011). Scoping study on pseudolites. *JRC Scientific and Technical Reports, European Commission*, 20.

PCTEL (2021). Coach™ ii 5G cellular GNSS multiband antenna. `https://d3dqzy9ky05fbv.cloudfront.net/wp-content/uploads/2020/06/GL125-DLTEMIMO-SM.pdf`. Last accessed: 26-09-2022.

Serrano, J., Lipinski, M., Wlostowski, T., Gousiou, E., van der Bij, E., Cattin, M., and Daniluk, G. (2013). The white rabbit project.

SSB-Electronic-GmbH (2023). Aircell 7.